# Precise source location of AE doublets by spectral matrix analysis of triaxial hodogram

# Precise source location of AE doublets by spectral matrix analysis of triaxial hodogram

Hirokazu Moriya*, Koji Nagano*, and Hiroaki Niitsuma*

## ABSTRACT

We have developed a precise relative source location technique using acoustic emission doublets (AE doublets) in the triaxial hodogram method to evaluate the direction and distance of subsurface extension cracks. An AE doublet is a pair of acoustic emissions with similar waveforms and adjacent locations on the same crack but which occur at different times. The relative source location is estimated by an analysis in the frequency domain. The relative distance between two AE sources is determined from the difference of $P$-$S$ arrival time delays by cross-spectrum analysis. The relative direction is derived using a spectral matrix from the difference in $P$-wave polarization directions. We also propose a method to optimize the estimated relative location by using a group of AE doublets.

The accuracy of the estimated source location was confirmed by performing field experiments. The relative locations of artificial wave sources about 150 m from a triaxial detector can be estimated with distance errors of less than 1 m, and direction errors of less than 3.8 degrees in both azimuth and inclination. Results of the application of this analysis on AE doublets in a geothermal field demonstrate its ability to evaluate deeper subsurface fractures.

## INTRODUCTION

Monitoring and assessing subsurface cracks has recently become quite important because of the accelerated progress of underground exploitation, such as geothermal energy extraction and construction of radioactive waste storage sites.

The downhole acoustic emission (AE) method provides information concerning the dynamic behavior of active subsurface cracks, and is being used in several subsurface

applications. For example, hydraulically induced cracks have been measured and located by AE analysis in hot dry rock geothermal projects (Albright and Pearson, 1982; Baria and Green, 1986). Measurement and control of the geothermal crack reservoir has been successfully performed in a hydrothermal area by employing the downhole AE technique (Niitsuma et al., 1987).

Estimation of an AE source location is a fundamental technique to monitor the dynamic behavior of subsurface fractures. Two types of source location methods have been applied to subsurface AE measurements. One approach is the single-component transducer array, where the traveltime differences for AE waves to the elements of the array are analyzed. The other approach is the triaxial hodogram method, where the $P$-wave arrival direction and the $P$-$S$ arrival time delay are measured from a signal recorded by a downhole triaxial detector (Albright and Pearson, 1982). This triaxial hodogram method makes it possible to determine AE source locations by single-hole instrumentation. This advantage enables us to measure deeper subsurface cracks, for instance in geothermal fields, where it is difficult to establish multiple observation sites.

Source location methods can also be categorized into absolute location and relative location types. The absolute location method estimates the individual locations of seismic sources. However, the accuracy of the absolute source location in the triaxial hodogram method is not satisfactory if we intend to use the AE data to determine a drilling target or to recognize three-dimensional (3-D) configurations of fractures, etc. This is because small detection errors caused by background noise greatly affect the estimation of the AE source location.

Poupinet et al. (1984) have proposed a precise method of estimating the relative source location using arrival-time delays. They identified earthquake doublets as a pair of similar earthquakes originating from stress release on the same part of the fault (Geller and Mueller, 1980). The relative distance between two sources was represented by the difference of $P$-wave arrival time minus the difference

between the origin times of the two events (Poupinet et al., 1984). They detected the time delay between two seismograms using the cross-spectrum method and accurately estimated the relative distance. Errors were on the order of 10 m even though the location of the earthquake doublets was 10 to 50 km from their observation sites. The feasibility of this method was demonstrated by identifying the source locations for earthquakes on the Calaveras fault in California.

Using downhole AE measurement, we can also identify AE events that resemble each other. It can be postulated that the source mechanisms and locations of these events are almost identical and the seismic path properties, such as attenuation and scattering, are also similar. If the precise relative source location method can be combined with the triaxial hodogram method, we will be able to reveal subsurface crack extension behaviors. This technology could be used in various underground developments.

In this paper, we propose a procedure for processing AE doublet signals using the triaxial hodogram method to estimate the precise relative source location. First we discuss cross-spectrum analysis for measuring relative distance and describe the procedure for estimating relative direction using the spectral matrix. We also propose a method for optimizing relative source location estimates. Finally, we demonstrate the feasibility of these methods by showing some results obtained using an artificial seismic source and AE doublets observed in a geothermal field.

## CONCEPT OF AE DOUBLET ANALYSIS USING THE TRIAXIAL HODOGRAM METHOD

### AE doublets

AE events with similar waveforms and high correlation to each other, in spite of different origination times, are called "AE doublets" and are associated with earthquake doublets (Poupinet et al., 1984). Figure 1 shows typical three-component waveforms of AE doublets that were detected by downhole triaxial measurement in the Kakkonda geothermal field, Iwate prefecture, Japan (Niitsuma et al., 1987). It is postulated that AE doublets have identical source mechanisms. Furthermore, because of the adjacent seismic source location, the properties of the wave-propagation medium are believed to be almost identical. Therefore, AE doublets seem to be the expression of stress release on the same part of an active subsurface crack. The method of analysis of AE doublets in this paper is applied to a pair or a group of such events to reveal subsurface crack behaviors by estimating their precise relative source locations.

### Relative source location of doublets

Figure 2 explains the concept of relative source location used with our triaxial hodogram analysis. In the doublet analysis, the relative distance ($\Delta L = 1_a - 1_b$) and the relative direction [$\Delta\theta$ (horizontal angle), $\Delta\phi$ (vertical angle)] must be estimated.
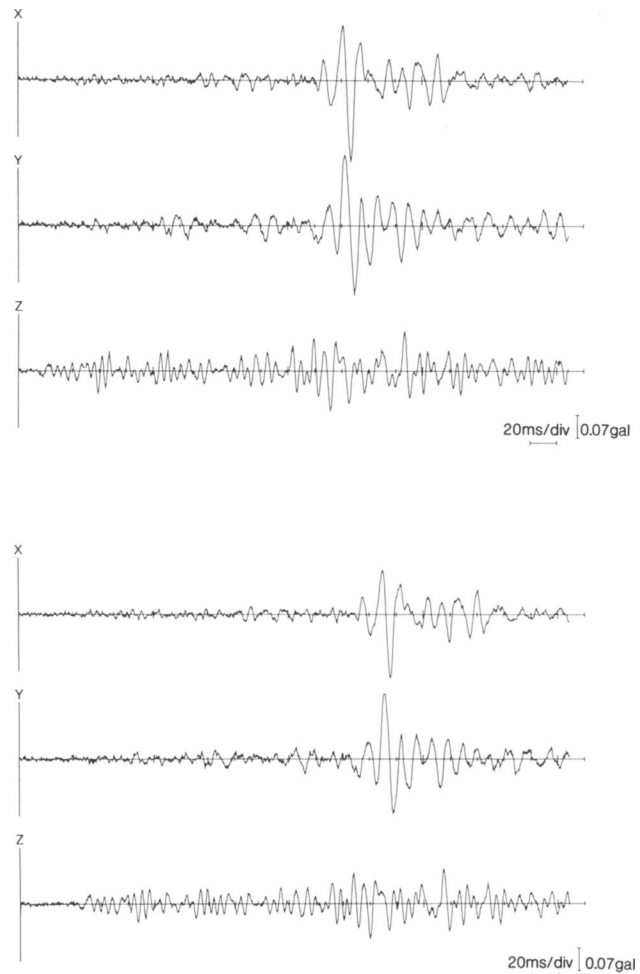


FIG. 1. Typical three-component waveforms of AE doublets observed in Kakkonda geothermal field.
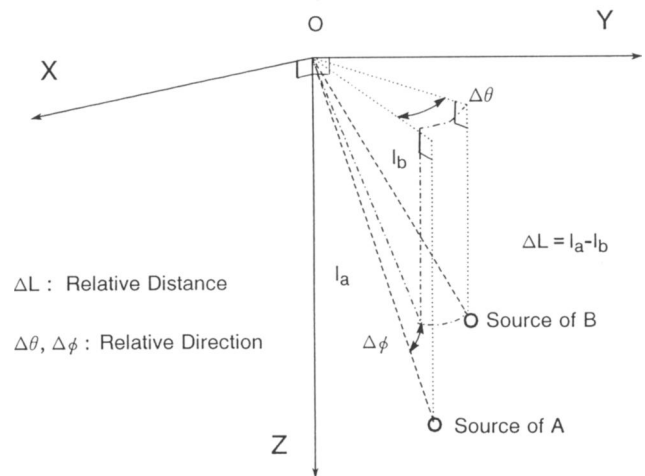


FIG. 2. Concept of relative source location used with triaxial hodogram analysis.

The relative distance is

$$\Delta L = \ell_a - \ell_b = \frac{(t_{sa} - t_{pa}) - (t_{sb} - t_{pb})}{\dfrac{1}{V_S} - \dfrac{1}{V_P}}$$

$$= \frac{\Delta_S - \Delta_P}{\dfrac{1}{V_S} - \dfrac{1}{V_P}}, \qquad (1)$$

where

$$\Delta_P = t_{pa} - t_{pb}, \quad \Delta_S = t_{sa} - t_{sb} . \qquad (2)$$

The arrival times of $P$- and $S$-waves are denoted by $t_{pi}$ and $t_{si}$ ($i = a, b$), and $V_P$ and $V_S$ are the velocities of $P$- and $S$-waves, respectively. According to equation (1), the relative distance $\Delta L$ is represented by the difference of $P$-$S$ arrival-time delays between the doublets, that is $\Delta_s - \Delta_P$.

On the other hand, the relative directions $\Delta\theta$ and $\Delta\phi$ are determined from the difference of $P$-wave incident directions into the triaxial detector. The source direction coincides with the directions of $P$-wave propagation if we assume a homogeneous medium. The relative direction can then be provided by the difference in the $P$-wave polarization directions.

## ESTIMATION OF RELATIVE DISTANCE

### Detection of time delay by cross-spectrum analysis

The difference of $P$-$S$ arrival-time delays between two AE events provides the relative distance that is estimated by making use of the cross-spectrum and the spectral coherence.

Figure 3 is a flow chart of the cross-spectrum analysis. Suppose $a(t)$ and $b(t)$ ($t = n\tau$; $n = 0, 1, \ldots, N - 1$) are the windowed finite data of two triaxial signals in the time domain, where $\tau$ is the sampling interval and $N\tau$ is the length of the time series. If $A(f)$ and $B(f)$ are the Fourier transforms of $a(t)$ and $b(t)$, the spectral density functions are

$$S_{aa}(f) = A(f)A(f)^*, \quad S_{bb}(f) = B(f)B(f)^*, \qquad (3)$$

and

$$\mathbf{S}_{ab}(f) = A(f)B(f)^* = K_{ab}(f) - jQ_{ab}(f), \qquad (4)$$

where $S_{aa}(f)$ and $S_{bb}(f)$ are the power spectra, and $\mathbf{S}_{ab}(f)$ is the cross spectrum. The cross-spectrum is represented by the cospectrum $K_{ab}(f)$ and the quadrature spectrum $Q_{ab}(f)$. The asterisks in the equations denote the complex conjugate.

From these two spectral density functions, the phase and the coherence, which is the normalized cross-spectrum, are

$$\psi(f) = \tan^{-1}\left(\frac{Q_{ab}(f)}{K_{ab}(f)}\right), \qquad (5)$$

and

$$Coh^2(f) = \frac{|\mathbf{S}_{ab}(f)|^2}{S_{aa}(f)S_{bb}(f)} , \qquad (6)$$

respectively. The delay between the two windowed signals is then a function of frequency given by the gradient of phase with frequency, that is

$$\Delta(f) = \frac{\psi(f)}{2\pi f} . \qquad (7)$$

The coherence is a measure of the crosscorrelation between two variable processes and is primarily used to detect common frequency components on two different signals. The time delay [$\Delta(f)$] can be precisely estimated by using both the phase and the coherence because it can be evaluated after recognizing AE components with high coherence.

The time delay detection in the frequency domain has the following advantages for suppressing the estimation errors caused by the resonance of the triaxial detector and background noise: (1) A frequency range with a high correlation between doublets can be recognized by referring to the coherence. This feature makes it possible to distinguish AE components from background noise in the frequency domain. (2) Time delay can be detected very precisely by evaluating the derivative of $\psi(f)$ over the detected frequency range.
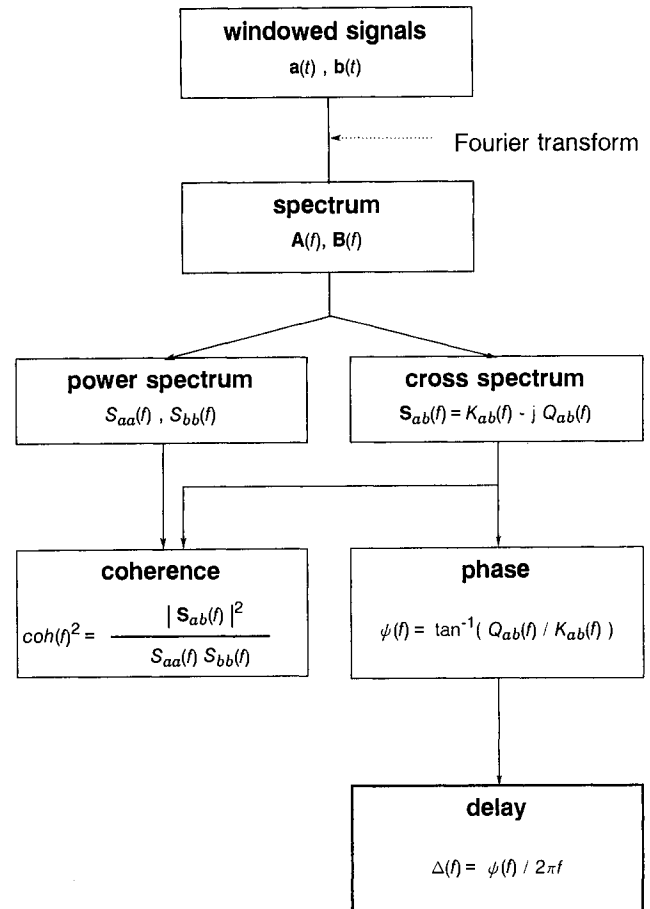


FIG. 3. Flow chart of cross-spectrum analysis.

## Estimation of the difference of *P-S* arrival-time delays

We use the cross-spectrum to evaluate time delay by observing highly correlated frequency components between the doublets. Through cross-spectrum analysis of *P*- and *S*-wave onsets, the *P*- and *S*-wave delay [$\Delta_P$ and $\Delta_S$ in equation (2)] can be obtained. Before estimating the time delay, we transform the coordinates of the three component signals $x(t)$, $y(t)$, and $z(t)$ into $p(t)$, $sh(t)$, and $sv(t)$ components. The signal $p(t)$ is the component of the *p*-axis corresponding to the *P*-wave arrival direction, $sh(t)$ is the component of the *sh*-axis that lies on the horizontal plane and is orthogonal to the *p*-axis, and $sv(t)$ is the component orthogonal to both the *p*- and *sh*-axes. The cross-spectrum analysis is independently applied to $p(t)$ and $sh(t)$ to estimate the *P*- and *S*-wave time delay. After obtaining $\Delta_S - \Delta_P$, the relative distance for the AE doublets is derived using equation (1).

## Example

We illustrate this method of determining the relative distance using the AE doublets shown in Figure 1. Figure 4 shows the time delay $\Delta(f)$ and the coherence for the *P*-wave onset window, where the waveforms $\mathbf{a}(t)$ and $\mathbf{b}(t)$ described in the figure are the *p*-axis components of the AE signals. The rectangular time windows in Figure 4 designate the regions for the cross-spectrum calculation, with $N = 300$ and $\tau = 0.2$ ms. The coherence has a peak in the frequency range of 50–125 Hz, where the dominant component of the *P*-wave exists. In accordance with the high coherency, the time

delay is stable within this frequency range; therefore, we can determine a time delay between two windowed signals as a average value over the frequency range where the spectral coherence has a higher level, resulting in a suppression of estimation errors caused by background noise. For this example, the time delay is determined to be 5.91 ms within the interval 50 to 125 Hz.

The change of the time delay as the individual windows slide along the components of the *p*- and *sh*-axes is described in Figure 5. The time delay is nearly stable throughout the entire region, even though there are minor fluctuations of less than 1 ms that are believed to be caused by multiple arrivals. Since the change of the estimated time delay is so small, both the *P*- and *S*-wave time delay can be reasonably determined from the average of the *P*- and *S*-wave (*SH*) onsets. The *P*-wave delay ($\Delta_P$) is evaluated as 6.03 ms and the *S*-wave delay ($\Delta_S$) is 6.52 ms. The difference for the *P-S* arrival-time delay ($\Delta_S - \Delta_P$) between the doublets is 0.49 ms and the relative distance ($\Delta L$) is 2.4 m [equation (1); $V_P = 3560$ m/s, $V_S = 2060$ m/s]. For the doublet, the signal-to-noise ratio is 5 dB at the *P*-wave onset and is over 15 dB at the *S*-wave. The power is dominant in the frequency range of 50–100 Hz, and the bandwidth of the signal is narrow. By computing the time delay using least-squares errors of the delay for *P*- and *S*-waves, we can obtain time precision better than the digitizing rate of 0.2 ms. Therefore, this signal processing has the ability to measure the relative distance with a resolution less than 1.2 m. The distances from the detector to each AE doublet source are about 1 km.
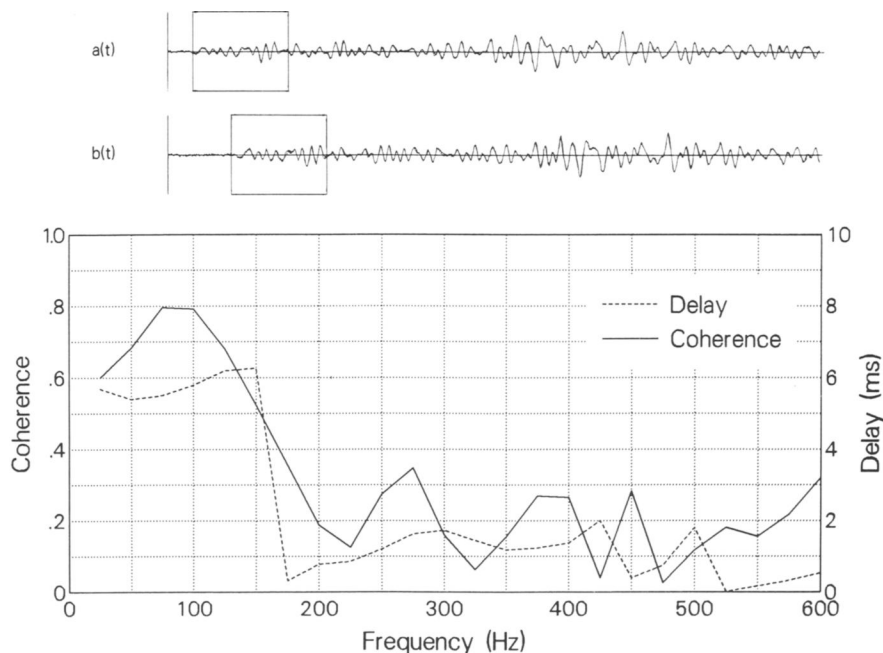


FIG. 4. Time delay and coherence for *P*-wave onset of the AE doublets shown in Figure 1. The waveforms $\mathbf{a}(t)$ and $\mathbf{b}(t)$ are the *p*-axis signals that correspond to the *P*-wave arrival direction.

## ESTIMATION OF RELATIVE DIRECTION

### Spectral matrix

Once the Fourier transforms of the three signal components are obtained, the spectral density functions are computed using equations (3) and (4). Hence, we can define the spectral matrix as

$$\underline{S}_p(f) = \begin{pmatrix} S_{xx}(f) & S_{xy}(f) & S_{xz}(f) \\ S_{yx}(f) & S_{yy}(f) & S_{yz}(f) \\ S_{zx}(f) & S_{zy}(f) & S_{zz}(f) \end{pmatrix}, \qquad (8)$$

where the diagonal terms $S_{ii}(f)$ ($i = x, y, z$) denote the power spectra, and the off-diagonal terms $S_{ij}(f)$ ($i, j = x, y, z, i \neq j$) are the cross spectra between three components (Samson, 1977). The spectral matrix is generally complex but always satisfies the condition of a Hermitian matrix, and may be considered a covariance matrix within the frequency domain. All of the information needed to characterize the wave polarization, i.e., principal direction and ellipticity, is contained in the spectral matrix, if the matrix consists of the spectra of 3-D wave data.

### Estimation of *P*-wave direction with the spectral matrix

Use of the spectral matrix in polarization analysis is feasible for the accurate detection of a *P*-wave arrival direction with triaxial AE measurement (Moriya et al., 1990). The *P*-wave direction as a function of frequency can be obtained by the eigenvalue analysis of the spectral matrix for *P*-wave onsets.

The spectral matrix satisfies the relationship

$$\underline{S}_p(f)\mathbf{u}(f) = \lambda(f)\mathbf{u}(f), \qquad (9)$$

$$|\underline{S}_p(f) - \lambda(f)\underline{E}| = 0, \qquad (10)$$

where $\underline{E}$ denotes a unit matrix. Three orthogonal eigenvectors $\mathbf{u}_i(f)$ ($i = 1, 2, 3$) of size $3 \times 1$ and three eigenvalues $\lambda_i(f)$ ($\lambda_1(f) > \lambda_2(f) > \lambda_3(f)$) can be obtained, respectively, for *i*-components by solving the above equations.

The cross-spectrum involved in the spectral matrix generally involves a complex number. However, for *P*-wave onset analysis, the imaginary portion of the values can be set to zero because the phase shift is basically 0 or 180 degree between the three components of triaxial signals. *P*-wave direction, which constitutes the largest fraction of *P*-wave energy, is obtained as the first eigenvector $\mathbf{u}_1(f)$ in the frequency domain. Analysis using the spectral matrix makes it possible to distinguish the *P*-wave direction from the background noise and the effect of resonance in the triaxial detector.

### Detection of the difference of *P*-wave arrival directions

Assuming a homogeneous medium, the relative direction of the doublets can be defined as the difference in *P*-wave arrival directions. Consequently, the estimation of relative direction is replaced by the detection of the relative angle between the two first eigenvectors of the spectral matrices.

In the first step, we set a pair of time windows starting from the *P*-wave arrival times as follow,

$$\text{For doublet } A: \quad t_{pa} \leqq t \leqq t_{pa} + t_c, \qquad (11)$$

$$\text{For doublet } B: \quad t_{pb} \leqq t \leqq t_{pb} + t_c, \qquad (12)$$

where $t_{pa}$ and $t_{pb}$ denote the *P*-wave arrival time of the respective doublets. The constant $t_c$ is the window length $N\tau$ for the analysis. Substituting the spectral matrices cal-
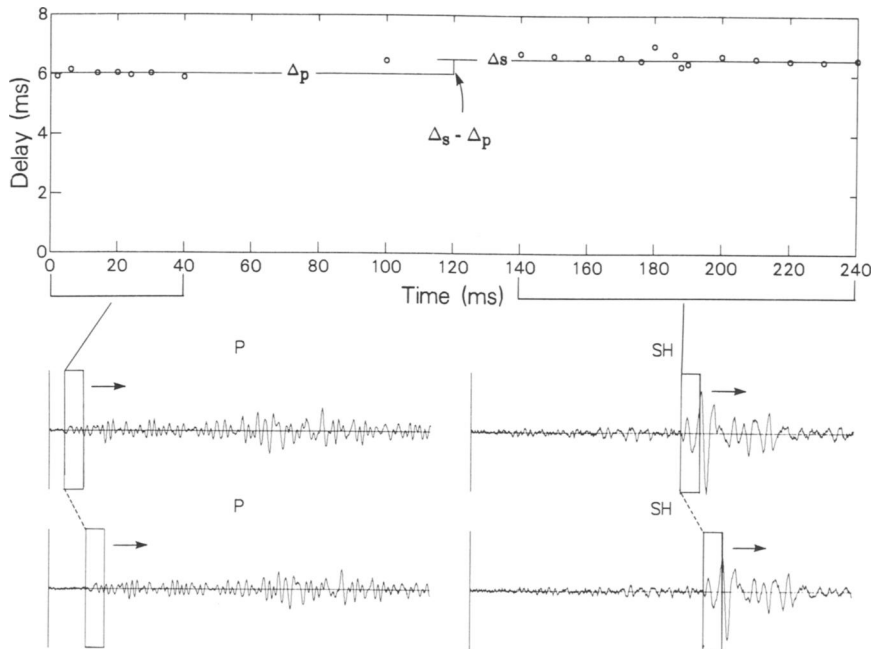


FIG. 5. Change of the time delay for individual time windows that slide on *p*- and *sh*-axes trace components. The $\Delta_p$ denotes the average of *P*-wave time delays, and $\Delta_s$ denotes the average of *S*-wave time delays.

culated in the time windows as, $\underline{S}_{pa}(f)$ and $\underline{S}_{pb}(f)$, individual equations are derived for each doublet:

For doublet $A$:  $\underline{S}_{pa}(f)\mathbf{u}_a(f) - \lambda_a(f)\mathbf{u}_a(f) = 0$    (13)

For doublet $B$:  $\underline{S}_{pb}(f)\mathbf{u}_b(f) - \lambda_b(f)\mathbf{u}_b(f) = 0$.    (14)

Designating $\mathbf{u}_{a1}(f)$ and $\mathbf{u}_{b1}(f)$ as the first eigenvectors in the solutions to these equations, the directions of the vectors $\mathbf{u}_{a1}(f)$ and $\mathbf{u}_{b1}(f)$ can be regarded as the arrival direction of the $P$-waves related to the AE doublet sources.

The relative angle of the two first eigenvectors can be derived by the following method. Let $\mathbf{u}_{b1}(f|\Delta\theta, \Delta\phi)$ be the vector of $\mathbf{u}_{b1}(f)$ rotated independently in azimuth ($\theta$) and inclination ($\Delta\phi$) on the $x$, $y$, $z$ orthogonal coordinate system. The residual errors $\mathbf{u}_{a1,k}(f) - \mathbf{u}_{b1,k}(f|\Delta\theta, \Delta\phi)$ represent a pair of constant-length time windows around the $P$-wave onsets that are synchronously advanced in time. The sum of the squared residuals of the sliding windows is

$$\varepsilon(f|\Delta\theta,\ \Delta\phi) = \frac{1}{M}\sum_{k=1}^{M}\|\mathbf{u}_{a1,k}(f) - \mathbf{u}_{b1,k}(f|\Delta\theta,\ \Delta\phi)\|^2, \quad (15)$$

where $M$ is the number of residual vectors, and $\mathbf{u}_{a1,k}(f) - \mathbf{u}_{b1,k}(f|\Delta\theta,\ \Delta\phi)$ is the residual vector at window $k$.

We can treat $\varepsilon(f|\Delta\theta, \Delta\phi)$ as a multiple-valued function of $\Delta\theta$ and $\Delta\phi$ with a fixed frequency. A rotation angle described by $\Delta\theta$ and $\Delta\phi$ minimizes $\varepsilon(f|\Delta\theta, \Delta\phi)$ if it corresponds to the relative direction of the AE doublet source. Estimates of the relative direction ($\Delta\theta$ and $\Delta\phi$) can be determined by a direct comparative method, such as the sequential simplex search (Stone, 1975).

### Example

We can use the following signal processing method to determine the relative direction of the doublets shown in Figure 1. Since the dominant components of the signals exist around 100 Hz, we consider only a 20 ms window length ($t_c$) of the 100 Hz component, which corresponds to twice the signal period, where $N = 100$ and $\tau = 0.2$ ms. Figure 6 shows the estimated relative directions and the residual errors as a function of $M$ in equation (15). The simplex method was used to find the rotation angles that minimize the residual error defined in equation (15). The residual errors in Figure 6 have a minimum at $M = 4$, and the estimated directions are less stable when $M$ is greater than 7. The residual errors when $M < 4$ are caused by background noise. On the other hand, the residual error increase corresponding to the increases of $M$ represents the incidence of multiple arrivals, where the estimated azimuth suddenly changes. Since the residual error is an indication of the accuracy of the estimation, the rotation angle at $M = 4$ may be adopted as a reliable estimate of the relative direction. The estimated relative direction of the doublets is 6 degrees in azimuth and 1 degree in inclination. Based on the absolute source direction of the first event ($\theta = 0.9$ degrees, $\phi = 82.5$ degrees), the direction of the second event is deduced as ($\theta = 6.9$ degees, $\phi = 83.5$ degrees).

### OPTIMIZATION OF ESTIMATED RELATIVE LOCATION

Groups of AEs that can be regarded as combinations of AE doublet events are often observed in field AE measurements. Estimates of the relative source locations for all

combinations of AE events can be evaluated by using both cross-spectrum and spectral matrix analysis. The least-squares method can be used to derive an optimum estimate of the relative source locations.

Suppose that there are $N$ AE events ($N \geq 3$), and that we want to optimize the relative source location between events $i$ and $j$ ($i, j = 1, 2, \cdots, N; i \neq j$). We first use the detected parameters of events $i$, $j$, and $k$ event ($k = 1, 2, \cdots, N; k \neq i, j$) in the following vectors $(\Delta L_{ik}, \Delta\theta_{ik}, \Delta\phi_{ik})^t$ and $(\Delta L_{jk}, \Delta\theta_{jk}, \Delta\phi_{jk})^t$. If $(\Delta L_{ij}, \Delta\theta_{ij}, \Delta\phi_{ij})^t$ is an optimal estimate of the relative source location between $i$ and $j$ events, then

$$\begin{pmatrix} \Delta L_{ik} - \Delta L_{jk} \\ \Delta\theta_{ik} - \Delta\theta_{jk} \\ \Delta\phi_{ik} - \Delta\phi_{jk} \end{pmatrix} = \begin{pmatrix} \Delta L_{ij} \\ \Delta\theta_{ij} \\ \Delta\phi_{ij} \end{pmatrix} + \begin{pmatrix} e_{\Delta L,k} \\ e_{\Delta\theta,k} \\ e_{\Delta\phi,k} \end{pmatrix}, \quad (16)$$

where $(e_{\Delta L,k}, e_{\Delta\theta,k}, e_{\Delta\phi,k})^t = \mathbf{e}_k$ is an error vector. Equation (16) states that the optimum relative source location between the $i$ and $j$ events is represented by the detected relative locations that are provided by monitoring the $k$ event and the errors.
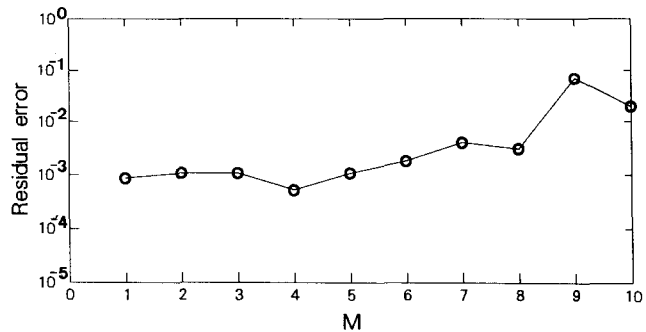
Considering the error vector in equation (16), we introduce the residual sum of squares as

$$\varepsilon_{ij} = \sum_{k=1}^{N}|e_k|^2. \quad (17)$$

Because the three parameters, distance, azimuth and inclination, are independent, the optimal solutions minimizing equation (17) are derived as
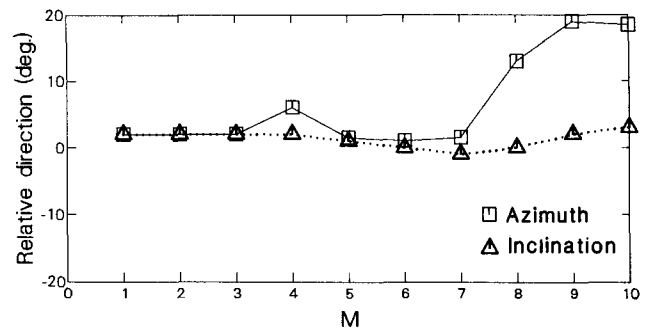


(a)



(b)

Fig. 6. Estimated relative direction and residual errors. (a) Estimated relative direction and (b) residual error. The $M$ is the number of residual vectors defined in equation (15).

$$\Delta L_{ij} = \frac{1}{N} \sum_{k=1}^{N} (\Delta L_{ik} - \Delta L_{jk}), \qquad (18)$$

$$\Delta \theta_{ij} = \frac{1}{N} \sum_{k=1}^{N} (\Delta \theta_{ik} - \Delta \theta_{jk}), \qquad (19)$$

$$\Delta \phi_{ij} = \frac{1}{N} \sum_{k=1}^{N} (\Delta \phi_{ik} - \Delta \phi_{jk}). \qquad (20)$$

Optimization of the other doublet combinations can be derived in a similar manner.

### ESTIMATION OF ARTIFICIAL WAVE SOURCE

An experiment was conducted at Higashi Hachimantai Field (Niitsuma, 1989) of Tohoku University, Iwate Prefecture, Japan, to verify the precision and the effectiveness of the doublet analysis. The field has six boreholes drilled into the intact welded tuff and is suitable for quantitative evaluations of doublet analysis; there are no significant natural fractures or joints, and the velocity structure has been clarified by calibration tests.

The experiment was performed using a downhole air gun as the artificial seismic source. To acquire wave data having similar waveforms that could be treated as doublets, the downhole air gun was shot at several adjacent levels. A triaxial AE sonde (Niitsuma et al., 1987) was employed as a detector. The sonde consisted of triaxial piezoelectric accelerometers, preamplifiers, an electric compass, and mechanical arms driven by gear motors. By using the sonde, triaxial particle motion of the wave can be detected at a frequency range of 7–400 Hz (Niitsuma et al., 1991; Nagashima et al., 1992). In the experiments, the sonde was clamped at 205.8 m in another borehole about 89 m horizontally from the borehole with the air gun. The detected signals were digitized with a 20 kHz sampling rate.

Figure 7 shows the waveform of the downhole air gun detected by the triaxial detector. Two waves have high correlation when the air gun is operated at slightly different depths. Thereforth, we treat the acquired set of data as doublets.

The actual locations of the air gun and the estimated relative distance for one of the experiments are summarized in Tables 1 and 2. When the air gun was shot at depths of 344 m and 351 m, the respective straight-line distances between the seismic source and the detector were 147.4 m and 153.5 m. The difference of $P$-$S$ arrival-time delay was detected as $-1.45$ ms. Using $V_p = 3183$ m/s and $V_s = 1681$ m/s which are the known wave velocities in this field, the relative distance is determined from cross-spectrum analysis as $-5.2$ m. Since the actual relative distance was $-6.1$ m, the estimation error is 0.9 m, which is 0.6 percent of the absolute distance from the source to the detector.

We also estimated the relative direction of the source from the following methods using both conventional analysis and our proposed analysis: (a) estimation from the absolute directions determined by conventional triaxial hodogram analysis, (b) detection by the least-squares method using the time-series vectors of $P$-waves, (c) detection by the least-squares method, after preprocessing by an optimum filter that maximizes signal to noise ratio, (d) detection by the least-squares method, after preprocessing by a narrow band-pass filter (150 terms FIR filter) whose center frequency is determined by the coherency among three signal components of $P$-wave onset to ensure the $P$-wave components behave with linear particle motion, and (e) detection with the spectral matrix, where we consider only the frequency component of 100 Hz.

Estimated relative directions are shown in Table 3. In this experiment, the actual relative direction was 0.4 degree azimuth and 1.2 degree inclination. The estimated relative direction using spectral matrix analysis is much closer to the actual relative direction than with the results of other signal processing methods in the time domain. The result of (d) is equivalent to that of (e) because both signal processing methods only consider limited frequency components. We further examined the precision of the spectral matrix analysis by using the wave data obtained from operating the air gun at several different depths. Figure 8 shows the results of the estimation errors for 17 experiments. The deviations of the errors are almost within 3.8 degrees of both the azimuth and inclination.
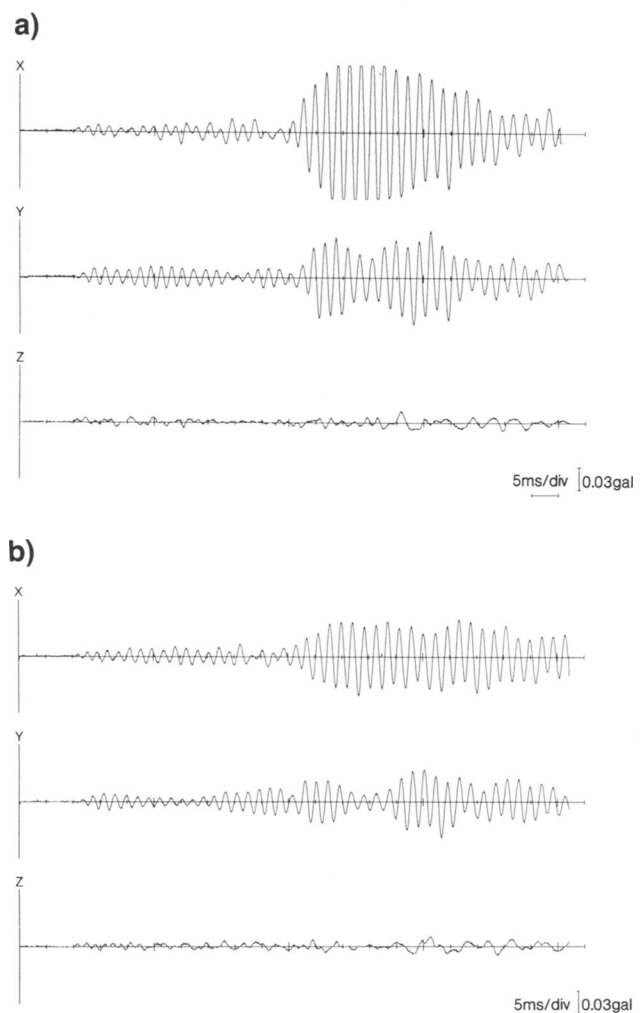
a)



b)



FIG. 7. Typical three component waveforms of downhole air gun.

## ESTIMATION OF AE EVENTS IN A GEOTHERMAL FIELD

We applied AE doublet analysis to events observed in Kakkonda geothermal field (Niitsuma et al., 1985), Iwate Prefecture, Japan. A 50 MWe geothermal electric power plant is operated in the field. A number of geothermal production wells are drilled into highly permeable fractured zones in the field.

We performed triaxial downhole AE measurements when a production well was being drilled (Takanohashi and Niitsuma, 1988). Figure 9 shows the locations of the production well and the triaxial detector, where the triangle designates the location of the downhole triaxial detector, and the curved line denotes the borehole locus of the production well. The downhole triaxial detector was set near the bottom of a shallow test borehole at a depth of 46.2 m.

Lost circulation of drilling fluid occurred during a slime elimination process at a depth of about 1341 m, which is designated by a cross in Figure 9. The change of flow rate of drilling fluid is shown in Figure 10 where AE activity is also shown. The lost circulation rate was 17 kl/h. These phenomena were understood as one kind of hydraulic fracturing, where the drilling fluid was lost into the formation creating an artificial fracture. About 40 AE events were observed in response to the lost circulation. Seven of them have similar waveforms and are identified as doublets. Figure 11 shows three examples of three-component waveforms of the AE

doublets. These AE events were detected within one and a half minutes, between 13:34:47 to 13:35:52 hours. Since these AE events were generated from the hydraulically induced fracturing within a very short time duration, these seven events are considered to have identical source mechanisms.

We located the sources of the AE doublets by using two methods: (1) estimation of the absolute source location method and (2) estimation of the relative source location method by doublet analysis and optimization. The results are shown in Figures 12a and 12b, respectively. The numbers in the figures designate the sequence of the events. The sources are estimated individually by conventional triaxial hodogram analysis in Figure 12a, where the P-wave arrival direction and the arrival time of P- and S-waves as picked by human observation were used. The sources of AEs No. 2 through No. 7 indicated in Figure 12b are the locations relative to the first event, No. 1, whose absolute location corresponds to the location in Figure 12a. The source locations derived using AE doublet analysis align and spread upwards. This mapping makes it possible to infer that the crack extended southeast over 100 m when the lost mud and water flowed into the natural discontinuity and activated the crack extension. It is known that distribution and direction of subsurface fractures are dominant to the northwest and southeast, and that vertical fractures are also dominant (Sato, 1982). The directions of the Neogene fold axes, which makes up the geothermal reservoir in the Kakkonda Field are also northwest and southeast. The direction of the crack extension estimated by the AE doublet analysis agrees well with the subsurface structure in this field. These results demonstrate the feasibility of AE doublet analysis using the spectral matrix and the cross-spectrum for evaluating deep subsurface crack behavior.

**Table 1. Actual location of downhole air gun.**

| Wave source | Distance (m) | Azimuth (deg.) | Inclination (deg.) | Relative distance (m) | Relative direction* (deg.) |
|---|---|---|---|---|---|
| A | 147.4 | 100.5 | 63.8 | −6.1 | (0.4, 1.2) |
| B | 153.5 | 100.9 | 65.0 | | |

*(Azimuth, Inclination)

**Table 2. Estimated time delays and relative distance.**

| $\Delta_p$ (ms) | $\Delta_s$ (ms) | $\Delta_s$-$\Delta_p$ (ms) | $\Delta L$ (ms) | Error (ms) |
|---|---|---|---|---|
| 0.21 | −1.24 | −1.45 | −5.2 | 0.9 |

**Table 3. Estimated relative directions using both conventional and proposed method.**

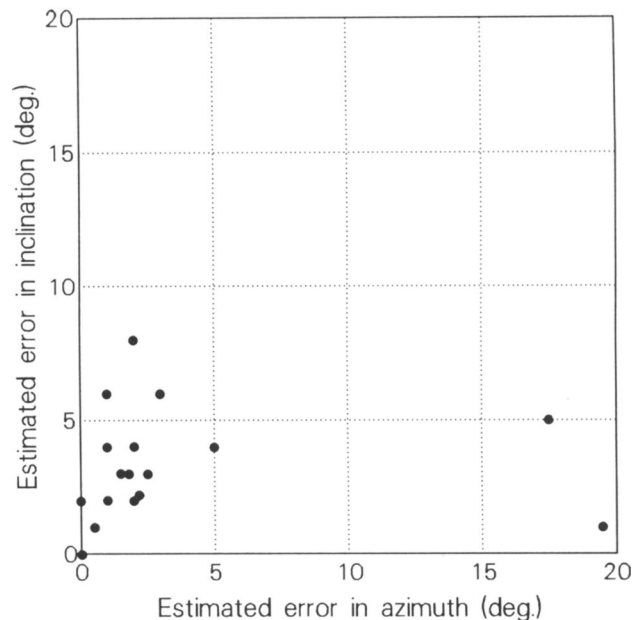| Processing | Estimated relative direction* (deg.) | Error* (deg.) |
|---|---|---|
| (a) Absolute source location | (−13.5, −7.4) | (13.9, 8.6) |
| (b) Relative source location (without filter) | (−10.0, −5.0) | (10.4, 6.2) |
| (c) Relative source location (optimum filter) | (9.5, −4.0) | (9.1, 5.2) |
| (d) Relative source location (filter based on coherence) | (2.5, −2.0) | (2.1, 3.2) |
| (e) Relative source location (spectral matrix) | (0.5, −3.0) | (0.1, 4.2) |

*(Azimuth, Inclination)



FIG. 8. Estimation errors of relative direction between two seismic sources. The air gun was shot at several neighboring levels in a borehole. Each dot denotes the estimation error when the relative directions for 17 different pairs of data were analyzed.

## CONCLUSIONS

AE doublet analysis in the triaxial hodogram method can be used for precise estimation of relative AE source locations. The relative distance of AE doublets can be derived by time delay estimation using cross-spectrum analysis employing coherence. Relative direction can be estimated from the difference of $P$-wave arrival directions using the spectral matrix. Based on artificial doublets generated by a downhole air gun, doublet analysis can determine relative distance with an error of less than 1 m and relative direction to within 3.8 degrees, as
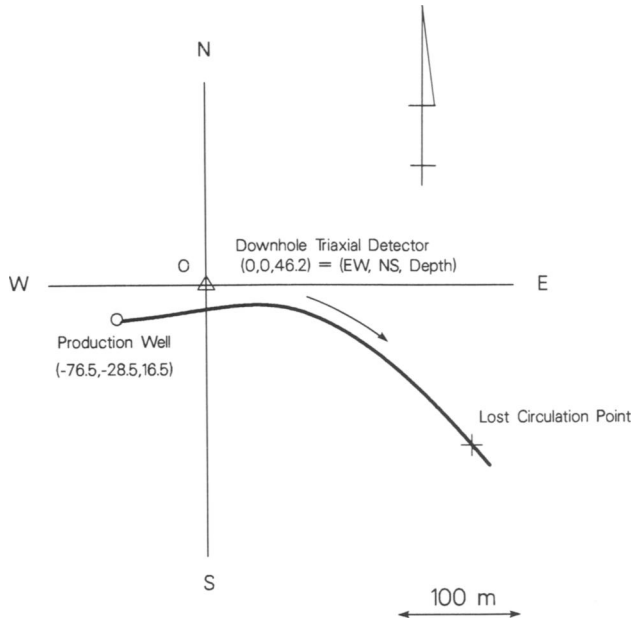
FIG. 9. Locations of production well and triaxial detector. Triangle designates location of downhole detector, where the downhole triaxial detector was set at a depth of 46.2 m in a shallow test borehole. Lost circulation of drilling fluid occurred at a depth of 1341 m, denoted by a cross.
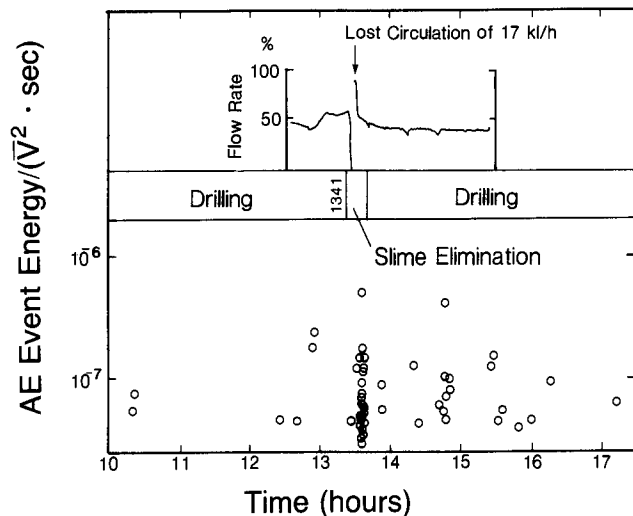
FIG. 10. Changes of flow rate of drilling fluid and AE activity.

a)

(a) No.1 13:34:47

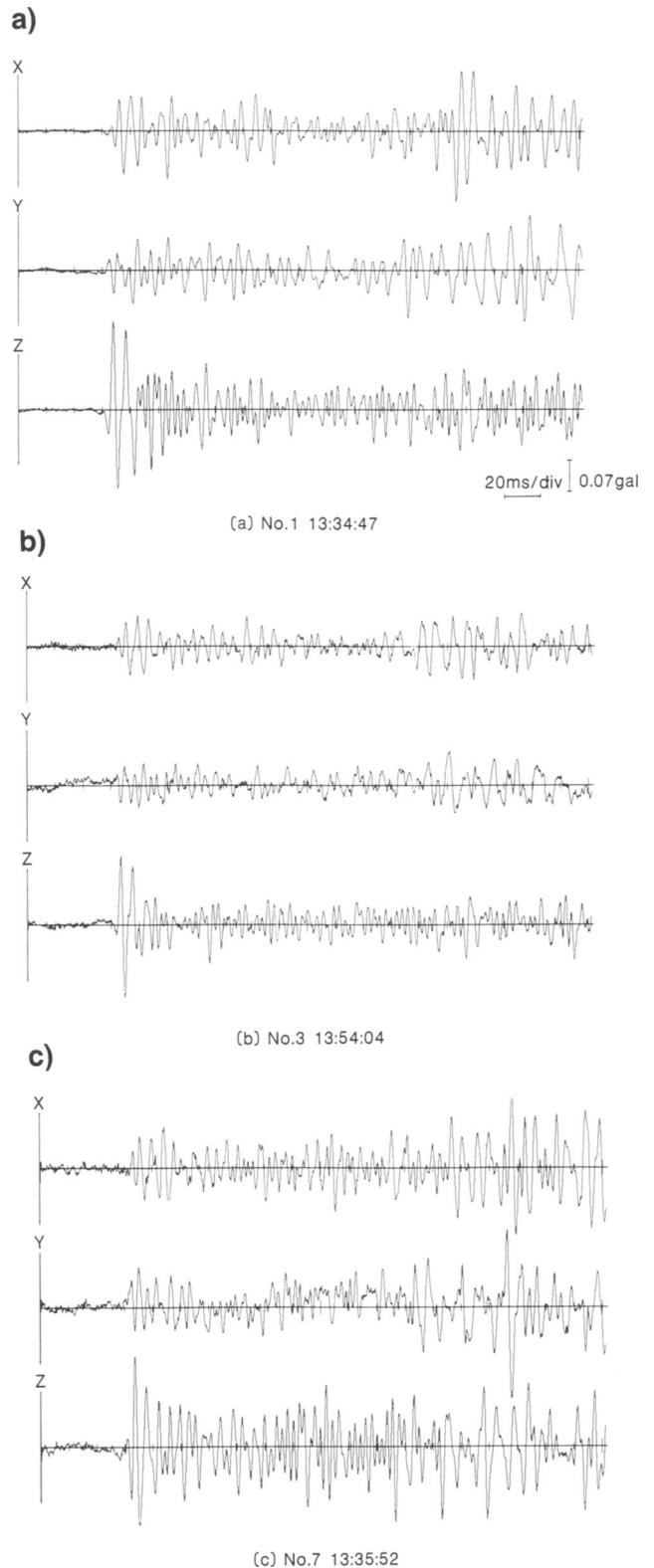b)

(b) No.3 13:54:04

c)

(c) No.7 13:35:52

FIG. 11. Examples of three-component waveforms of AE doublets. The numbers designate sequence of events.
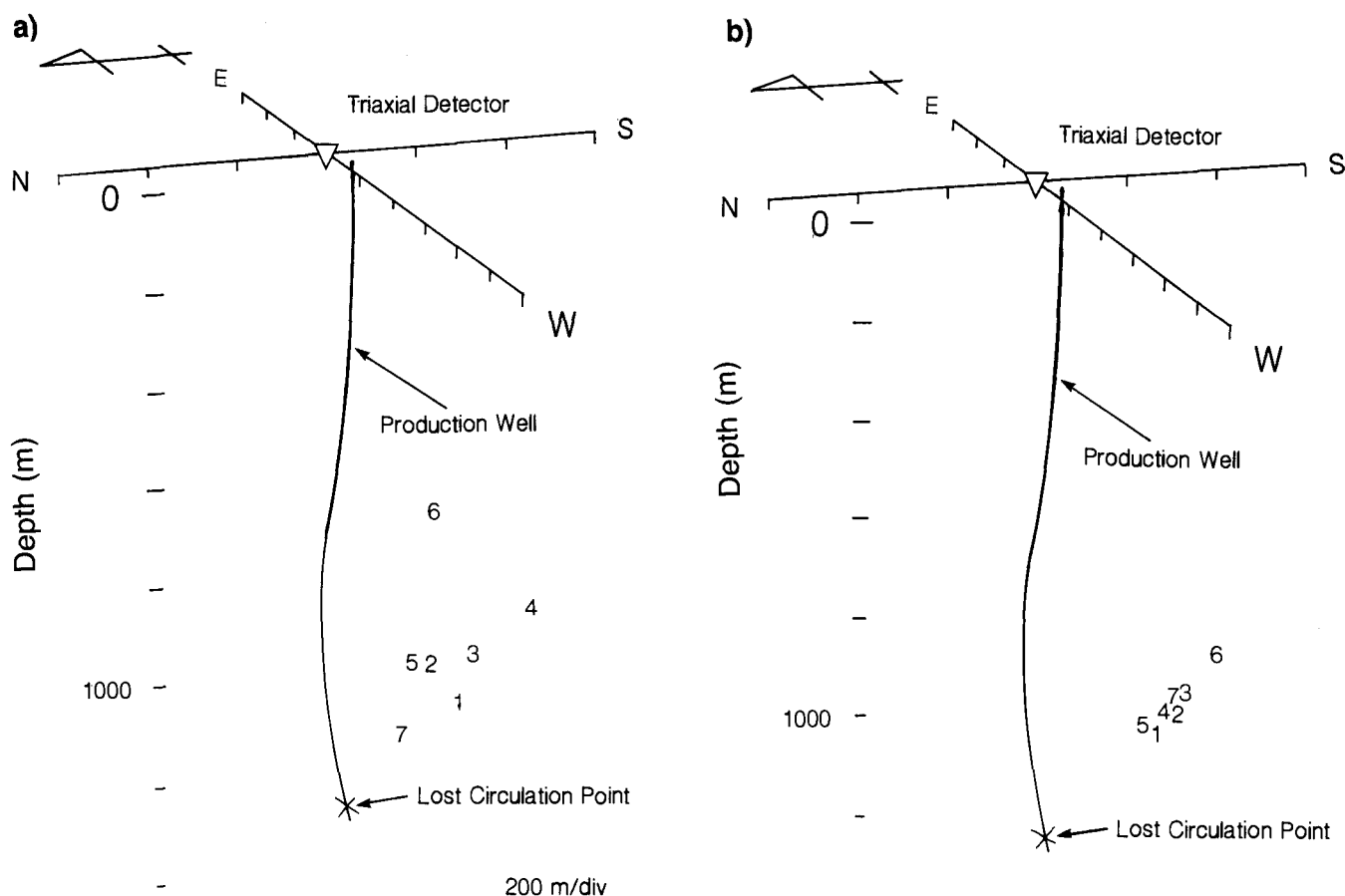
FIG. 12. Estimated AE source locations: (a) Conventional triaxial hodogram method and (b) AE doublet analysis. The indicated numbers designate the sequence of the events. Reference source in the relative source location is denoted by No. 1, and sources of No. 2–No. 7 are the locations relative to first event No. 1.

long as the downhole triaxial detector is about 150 m from the seismic source. The estimated relative source location can be optimized when multiple AE doublets are observed.

The direction of crack extension has been clearly revealed from the estimated AE doublets which were observed in a geothermal field. AE doublet analysis using the triaxial hodogram method is a practical technique for evaluating deep subsurface crack extension.

## REFERENCES

Albright, J. N., and Pearson, C. F., 1982, Acoustic emissions as a tool for hydraulic fracture location: Experience at the Fenton Hill Hot Dry Rock Site: Soc. Petr. Eng. J., 22, 523–530.

Baria, R., and Green, A. S., 1986, Seismicity induced during a viscous stimulation at the Camborne School of Mines hot dry rock geothermal energy project in Cornwall, England, in Yamaguchi, K., Aoki, K., and Kishi, T., Eds., Progress in acoustic emission III: The Japanese Soc. for NDI, 407–429.

Geller, R. J., and Mueller, C. S., 1980, Four similar earthquakes in central California: Geophys. Res. Lett., 7, 821–824.

Moriya, H., Nagano, K., and Niitsuma, H., 1990, Precise estimation of AE source direction by spectral matrix analysis, in Yamaguchi, K., Takahashi, H., and Niitsuma, H., Eds., Progress in acoustic emission V: The Japanese Soc. for NDI, 244–251.

Nagashima, S., Moriya, H., and Niitsuma, H., 1992, Development and calibration of downhole triaxial AE detector for subsurface and civil engineering AE measurements, in Kishi, T., Takahashi,

K., and Ohtsu, M., Ed., Progress in acoustic emission VI: The Japanese Soc. for NDI, 407–414.

Niitsuma, H., 1989, Fracture mechanics design and development of HDR reservoir—Concept and results of "T—Project": Internat. J. Rock Mech. and Min. Sci., Abstr. 26, 169–175.

Niitsuma, H., Chubachi, N., and Takanohashi, M., 1987, Acoustic emission analysis of a geothermal reservoir and its application to reservoir control: Geothermics, 16, 47–60.

Niitsuma, H., Moriya, H., and Nagano, K., 1991, Calibration method using the spectral matrix for downhole triaxial seismic detectors, in Hardy, H. R., Jr., Ed., Proc. 5th Conf. on Acoustic Emission/Microseismic activity in Geologic Structures and Materials, Penn. State University, (in press).

Niitsuma, H., Nakatsuka, K., Takahashi, H., Chubachi, N., Yokoyama, H., and Takanohashi, M., 1985, Acoustic emission measurement of geothermal reservoir cracks in Takinoue (Kakkonda) Field, Japan: Geothermics, 14, 525–538.

Poupinet, G., Ellsworth, W. L., and Frechet, J., 1984, Monitoring velocity variations in the crust using earthquake doublets: An application to Calaveras Fault, California: J. Geophys. Res., 89, 5719–5713.

Samson, J. C., 1977, Matrix and stokes velocity representations of detectors for polarized waveforms: Theory, with some applications to teleseismic waves: Geophys. J. Roy. Astr. Soc., 51, 583–603.

Sato, K., 1982, Analysis of geological structure in the Takinoue geothermal area: J. Geother. Res. Soc. Japan, 3, 135–148.

Stone, L. D., 1975, Theory of optimal search: Academic Press Inc.

Takanohashi, M., and Niitsuma, H., 1988, Reservoir creation and control by utilizing acoustic emission technique: Proc. Geothermal Resources Council/Am. Soc. Mech. Engr. Symp. on Geothermal Energy ETCE, 409–414.